

ARTICLE OPEN

Engineering the breaking of time-reversal symmetry in gate-tunable hybrid ferromagnet/topological insulator heterostructures

Joon Sue Lee ^{1,2}, Anthony Richardella¹, Robert D. Fraleigh¹, Chao-xing Liu¹, Weiwei Zhao¹ and Nitin Samarth ¹

Studying the influence of broken time-reversal symmetry on topological materials is an important fundamental problem of current interest in condensed matter physics and its understanding could also provide a route toward proof-of-concept spintronic devices that exploit spin-textured topological states. Here we develop a new model quantum material for studying the effect of breaking time-reversal symmetry: a hybrid heterostructure wherein a ferromagnetic semiconductor $\text{Ga}_{1-x}\text{Mn}_x\text{As}$, with an out-of-plane component of magnetization, is cleanly interfaced with a topological insulator $(\text{Bi,Sb})_2(\text{Te,Se})_3$ by molecular beam epitaxy. Lateral electrical transport in this bilayer is dominated by conduction through $(\text{Bi,Sb})_2(\text{Te,Se})_3$ whose conductivity is a few orders of magnitude higher than that of highly resistive $\text{Ga}_{1-x}\text{Mn}_x\text{As}$. Electrical transport measurements in a top-gated heterostructure device reveal a crossover from weak antilocalization to weak localization as the temperature is lowered or as the chemical potential approaches the Dirac point. This is accompanied by a systematic emergence of an anomalous Hall effect. These results are interpreted in terms of the opening of a gap at the Dirac point due to exchange coupling between the topological insulator surface state and the ferromagnetic ordering in $\text{Ga}_{1-x}\text{Mn}_x\text{As}$. The experiments described here show that well-developed III-V ferromagnetic semiconductors could serve as valuable components of artificially designed quantum materials aimed at exploring the interplay between magnetism and topological phenomena.

npj Quantum Materials (2018)3:51; doi:10.1038/s41535-018-0123-2

INTRODUCTION

A three-dimensional (3D) topological insulator (TI) is characterized by surface states that are protected by time-reversal (TR) symmetry.^{1–4} The TR symmetry can be broken by doping a TI with magnetic atoms or interfacing a TI surface with a magnetic layer, causing an energy gap to open at the Dirac point.^{5–8} Unique quantum phenomena resulting from the broken TR symmetry have been proposed: such as a topological magneto-electric effect,⁵ an image magnetic monopole effect,⁹ topological Kerr and Faraday rotation,⁵ and the quantum anomalous Hall effect (AHE).¹⁰ Some of these phenomena have been demonstrated experimentally.^{11–14} The synthesis and characterization of a variety of magnetically doped 3D TIs with transition metals have been reported in this context.^{7,15–20} Angle-resolved photoemission spectroscopy (ARPES) has suggested evidence for the opening of a gap induced by breaking TR symmetry in magnetically doped TI systems,^{7,8,18,21} although recent studies point out an alternative mechanism for the gap seen in such studies.²² In addition, a spin-resolved ARPES experiment revealed a hedgehog-like spin texture in the modified surface state of Bi_2Se_3 films by Mn doping.²³ Manipulating the spin texture of the surface states in a TI could play an important role within the burgeoning field of “topological spintronics.”^{24–29}

In this paper, we break TR symmetry in the surface state of a TI by interfacing the surface with a ferromagnetic insulator (FMI) with perpendicular magnetization. The key advantage of a TI/FMI

heterostructure over magnetically doped TIs is the selective modification of one surface by an adjacent FMI. Magnetic proximity affects only the interfaced surface; thus magnetic properties or the resulting effects are free from the magnetism of the bulk or other surfaces of the TI layer. So far, several TI/FMI heterostructures have been experimentally reported using FMIs interfaced with TIs where the chemical potential is located in or near the conduction band.^{30–38} In many cases, the magnetic anisotropy of the FMI was in plane. Ideally, to induce a magnetic gap, it would be preferable to have an FMI whose magnetization is perpendicular to the TI surface. Weak localization (WL),^{31,38} suppression of weak antilocalization (WAL),³⁴ and induced AHE^{33,39} have been observed by interfacing a TI with an FMI or ferri-magnetic insulator with perpendicular magnetic anisotropy.³⁹ However, electronic transport evidence of a magnetic gap can be ambiguous when the chemical potential of the TI is fixed as in previous studies, especially in the bulk bands that are away from the Dirac point. Thus there remains an important context for realizing an electrically gated TI/FMI heterostructure with a clean interface, perpendicular magnetic anisotropy, and chemical potential in the bulk band gap. We note also that, to avoid a non-magnetic gap due to quantum tunneling between opposite surface states, the TI film needs to be thicker than the critical thickness for hybridization.⁴⁰ Here we demonstrate a new approach that meets all these conditions using a TI/FMI

¹Department of Physics and Materials Research Institute, The Pennsylvania State University, University Park, PA 16802, USA

Correspondence: Nitin Samarth (nsamarth@psu.edu)

²Present address: California NanoSystems Institute, University of California, Santa Barbara, CA 93106, USA

Received: 20 May 2018 Revised: 12 September 2018 Accepted: 18 September 2018

Published online: 19 October 2018

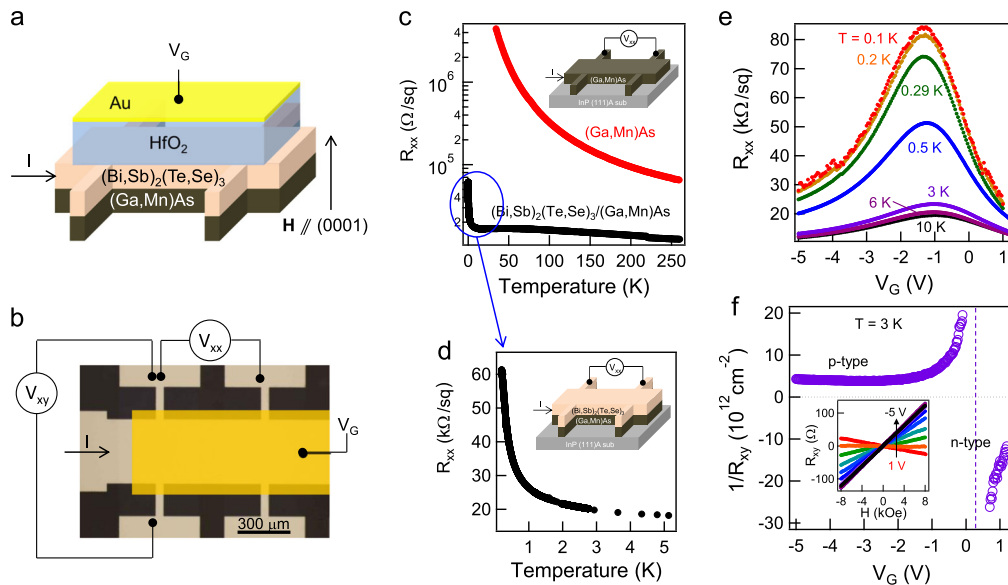


Fig. 1 Lateral electrical transport with temperature and gate-voltage sweep. **a** A schematic of a top-gated TI/(Ga,Mn)As Hall-bar device. **b** An optical microscopic image of a Hall-bar device ($650 \times 400 \mu\text{m}^2$) with false-colored Au gate metal and the measurement description. **c** Temperature dependence of the longitudinal sheet resistance R_{xx} of $(\text{Bi,Sb})_2(\text{Te,Se})_3/(\text{Ga,Mn})\text{As}$ heterostructure channel (black circles) and of only (Ga,Mn)As channel (red circles). Inset is a schematic of device and measurement description of (Ga,Mn)As layer. **d** R_{xx} of $(\text{Bi,Sb})_2(\text{Te,Se})_3/(\text{Ga,Mn})\text{As}$ heterostructure in the low temperature regime. Inset is a schematic of device and measurement description of the heterostructure. **e** Gate-voltage dependence of the longitudinal sheet resistance R_{xx} with zero magnetic field at different temperatures from 0.1 K (red) to 10 K (black). **f** Inverse of Hall resistance R_{xy} in the unit of 2D carrier concentration at 3 K. Inset is the results of Hall measurements with different gate voltages from 1 to -5 V at 3 K

heterostructure that uses a highly resistive III-V ferromagnetic semiconductor, (Ga,Mn)As, as the insulating ferromagnetic layer.

RESULTS AND DISCUSSIONS

Synthesis of $(\text{Bi,Sb})_2(\text{Te,Se})_3/(\text{Ga,Mn})\text{As}$ heterostructures

The ferromagnetic Curie temperature (T_C) and resistivity as well as the magnetic easy axis of (Ga,Mn)As films can be engineered by Mn-doping, annealing, and strain.^{41–43} Here we desire highly resistive $\text{Ga}_{1-x}\text{Mn}_x\text{As}$ with an out-of-plane magnetization. High resistivity was achieved by using a low Mn-doping of $x \approx 0.05$ and a perpendicular component of magnetization, with $T_C \approx 50$ K, by growing the (Ga,Mn)As film (15 nm) on an InP (111)A substrate by molecular beam epitaxy (MBE). (See Supplementary Information S1 for magnetic and structural characterization.) An advantage of using highly resistive (Ga,Mn)As for the TI/FMI heterostructure is the well-defined interface, without an amorphous interfacial layer or secondary phases, as was demonstrated for epitaxial growth of Bi-chalcogenide TIs on GaAs (111).⁴⁴ After growing the (Ga,Mn)As film, the substrate was transferred to another MBE chamber without breaking vacuum for the growth of the 3D TI $(\text{Bi,Sb})_2(\text{Te,Se})_3$ thin film (8 nm). The Dirac fermion dynamics in $\text{Bi}_2(\text{Te}_{3-x}\text{Se}_x)$ can be engineered by varying the composition of Te ($3-x$) and Se (x),⁴⁵ and we chose $x = 1$ ($\text{Bi}_2\text{Te}_2\text{Se}$) to place the Dirac point above the top of the valence band. The resulting elemental composition of Te and Se in the $(\text{Bi,Sb})_2(\text{Te,Se})_3$ film grown on the (Ga,Mn)As layer was Te:Se $\approx 2.1:0.9$, as determined by energy dispersive X-ray spectroscopy (EDS) in a transmission electron microscope (TEM). Further engineering of the chemical potential was achieved by Sb-doping: with an optimal ratio of Bi and Sb ($\text{Bi:Sb} \approx 1.25:0.75$), we were able to place the chemical potential in the bulk band gap, as confirmed by electrical transport measurements.

Ambipolar transport

Although the selective modification of one TI surface with an FMI is advantageous, as discussed earlier, the buried interface between

TI and FMI restricts direct probing of the modified TI surface state by techniques such as ARPES or scanning tunneling microscopy. However, electrical transport measurements do provide a route to study the modification of the surface states by quantum corrections to the magneto-conductance (MC) and via the AHE. For transport measurements, we fabricated a top-gated Hall-bar device with high- κ dielectric HfO_2 and Au/Ti gate metal by standard photo-lithography (Fig. 1a, b). One important question for the electrical transport laterally through the heterostructure is whether a current flows only through the TI layer. The black curve in the Fig. 1c, d represents the resistivity when the current flows through the whole TI/(Ga,Mn)As heterostructure while the red curve shows the resistivity of only the (Ga,Mn)As layer after the TI overlayer was carefully removed by mechanical scratching. Since the resistivity of the (Ga,Mn)As is more than two orders of magnitude higher than that of the bilayer <40 K and not even measurable at lower temperatures by standard direct current methods, we conclude that the current flows predominantly through the TI layer in the measurement range ($T \leq 3$ K) for studies of quantum corrections to MC and AHE; we can thus treat the (Ga, Mn)As layer as an FMI. Similar insulating behavior of the (Ga,Mn)As film was seen by selective removal of the TI overlayer using a low-power dry etch. We note that the InP substrate is semi-insulating and does not contribute to electronic transport at cryogenic temperatures.

The gate-voltage dependence of the longitudinal sheet resistance R_{xx} and Hall resistance R_{xy} of the TI/(Ga,Mn)As bilayer shows the typical ambipolar transport behavior of TI films (Fig. 1e, f). The Hall resistance R_{xy} changes sign at around $V_G = 0.3$ V while the longitudinal resistance R_{xx} reaches a maximum at $V_G = -1.3$ V. The mismatch of the gate voltages between the charge neutrality point, where the R_{xy} sign changes, and the R_{xx} peak reveals that the carrier densities of top and bottom surfaces do not match each other and the two surfaces could even have different types of carriers in a certain range of gate voltage. The chemical potential of the bottom surface state (interfaced with (Ga,Mn)As) may not be determined solely by the single-gate-voltage

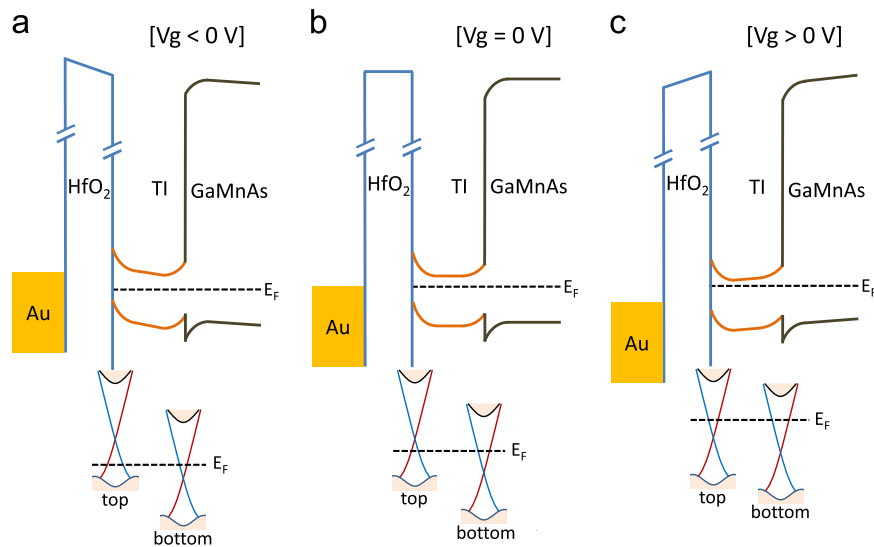


Fig. 2 Band alignment. Energy band alignment of the top-gated TI/(Ga,Mn)As heterostructure and band diagram of the top and bottom surfaces of the TI with gate-voltage tuning: **a** for $V_G < 0$ V, **b** for $V_G = 0$ V, and **c** for $V_G > 0$ V

dependence of the channel resistance and the Hall resistance of the whole TI layer. However, this chemical potential can be determined using careful studies of the quantum corrections to the MC and the AHE. Figure 2 illustrates the band alignment of the top-gated heterostructure and the chemical potential of the two surfaces with gate-voltage tuning, based on the ambipolar transport results and the MC and AHE studies that are discussed below. The band bending at the TI/(Ga,Mn)As interface arises from an estimated conduction band offset of about 1 eV. (See Supplementary Information S2 for more details.)

Quantum corrections to MC

We now discuss the results of magneto-transport measurements in a top-gated Hall-bar device as a function of both gate voltage and temperature (Fig. 3). At fixed temperatures of $T = 0.1$ K and $T = 0.29$ K, at a gate voltage $V_G = -5$ V, we observe a positive MC (Fig. 3a, b). As we decrease the magnitude of V_G toward zero and then increase it to $+1$ V, the positive MC gradually changes to a negative MC. One salient feature in the crossover regime is the coexistence of a negative MC peak near zero magnetic field and a positive MC for larger magnetic fields; this is more pronounced at $T = 0.29$ K. A similar crossover from positive MC to negative MC is also seen when we raise the temperature at a fixed gate voltage ($V_G = -5$ V) (Fig. 3c). The shape of the MC also changes as a function of temperature: as we increase the temperature from $T = 0.1$ K, the relatively sharp positive MC first transitions to a superposition of positive and negative MC. Then, at temperatures above $T \sim 3$ K, the MC shows a parabolic negative MC. The similarity for the crossovers in MC as a function of gate voltage and temperature suggest a unified underlying mechanism for both cases.

We interpret our observations using quantum corrections to the MC in a TI, taking into account diffusive transport in two parallel surface channels with different dephasing lengths, one with an intact Dirac point (preserved TR symmetry) and the other with a magnetic gap (broken TR symmetry).⁴⁶ The former refers to the top surface of the device and the latter to the bottom surface that is interfaced with the (Ga,Mn)As layer. For the top surface, the quantum corrections to diffusive transport result in a negative MC arising from WAL. (See Supplementary S3). For the bottom surface, the exchange interaction with the ferromagnetic (Ga,Mn)As layer is expected to lead to a magnetic gap (Δ). In this case, the

quantum corrections to the MC can result in either a negative MC due to WAL or a positive MC due to WL, depending on the ratio Δ/E_F , where E_F is the chemical potential. The crossover between WAL and WL essentially arises from the modification of the TI surface state $\varphi = \pi(1 - \Delta/2E_F)$.⁴⁶ When the ratio Δ/E_F is small, the Berry phase remains close to π , leading to WAL. When we increase the ratio by decreasing E_F using a gate voltage or by increasing the gap Δ by lowering temperature, the Berry phase approaches 0, leading to WL. This WAL–WL crossover in the MC has been experimentally demonstrated in temperature-dependent studies of MC in TI films with an energy gap opened by either hybridization or by magnetic doping/proximity.^{18,31,47–51} Our results show that this crossover can also be systematically engineered using a gate voltage and that it agrees qualitatively with the variation with temperature. Notably, in certain regimes of temperature and gate voltage, we observe the coexistence of a WAL peak near zero magnetic field and WL behavior at larger magnetic fields, agreeing with our model of at least two decoupled transport channels with different dephasing lengths. As the gate voltage is tuned from $V_G = -5$ V to $V_G = 1$ V at 0.29 K, the MC becomes positive (WL) for larger magnetic field while the negative WAL peak is still observed for small magnetic field near zero (Fig. 3b). We attribute the WL contribution to the MC to the gapped surface state of the bottom surface due to proximity with (Ga,Mn)As. The WAL peak near zero magnetic field arises from the gapless surface state of the top surface decoupled from the bottom surface.

To quantitatively analyze the WAL and WL, we fit the data by applying the theoretical expressions developed for the quantum corrections to the MC of a TI in the presence of a magnetic gap.⁴⁶ We note that, in our sample, the film is thick enough to prevent a hybridization gap created by tunnel coupling between the top and bottom surfaces. Further, in the range of gate voltage studied ($-5 \text{ V} \leq V_G \leq 1 \text{ V}$), the chemical potential of the TI always lies in the region where the bulk is depleted. This is indicated by the carrier density ($n_{2D} \cong 4.3 \times 10^{12} \text{ cm}^{-2}$) at $V_G = -5$ V, which is low enough to place the chemical potential in the bulk band gap. At $V_G = 1$ V, the chemical potential is still in the ambipolar transport region (Fig. 1f). Thus the top and bottom surfaces are completely decoupled and we describe the quantum corrections to the MC

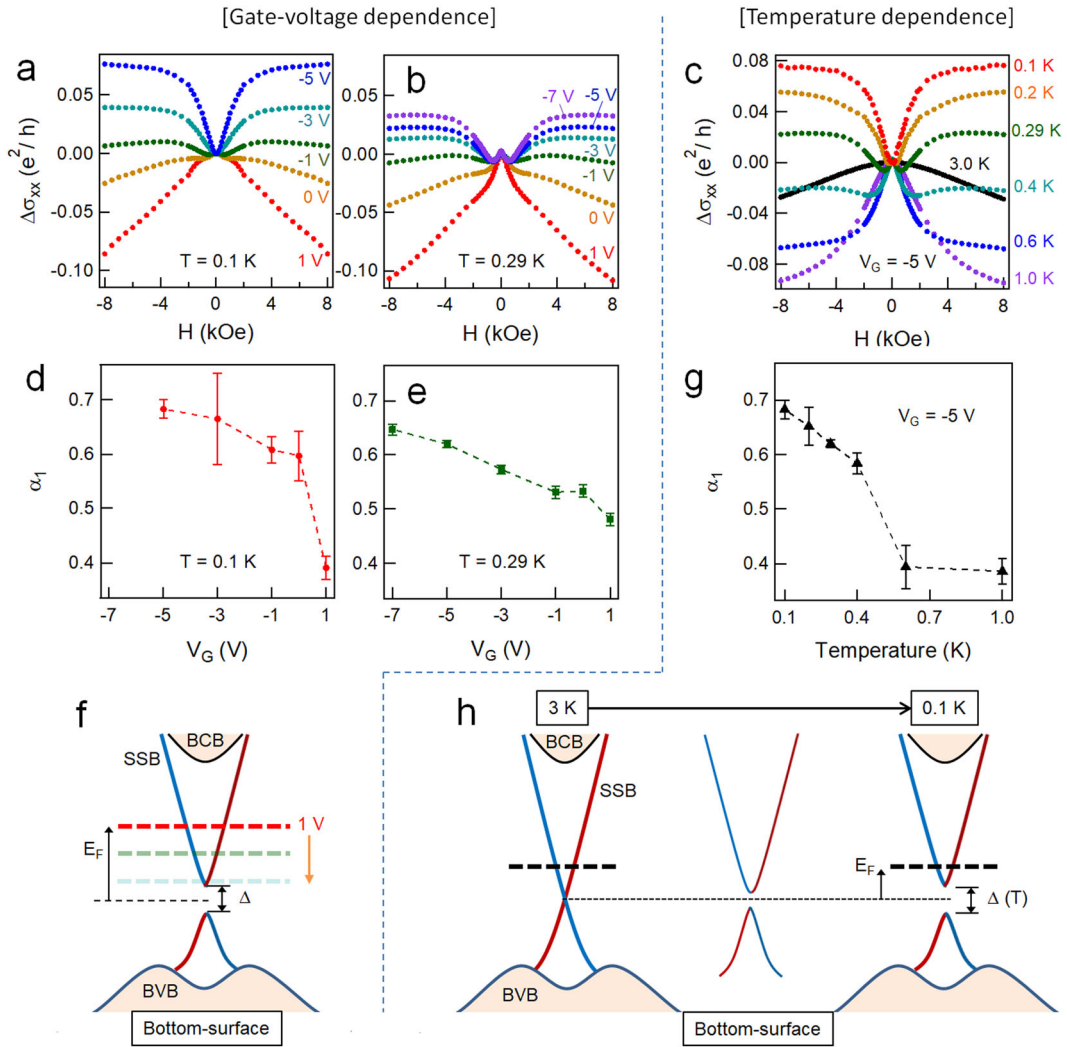


Fig. 3 Quantum corrections to MC. **a, b** MC at different applied gate voltage (V_G) at $T = 0.1$ K and $T = 0.29$ K, respectively. A crossover from negative MC (WAL) to positive MC (WL) is observed as V_G decreases from 1 to -5 V. **c** A similar crossover is observed in the temperature range 0.1–3.0 K at $V_G = -5$ V. **d, e** Gate-voltage dependence of the prefactor α_1 for the bottom surface obtained by fitting the MC in **d** at $T = 0.1$ K (red circles) and $T = 0.29$ K (green squares) to Eq. (1). **f** A cartoon of the band diagram of the bottom surface interfaced with (Ga,Mn)As. The magnetic gap (Δ) is fixed at a particular temperature as the chemical potential is varied from the conduction band toward the energy gap as the gate voltage decreases from $+1$ V toward -5 V. **g** Temperature dependence of the prefactor α_1 with $V_G = -5$ V (black triangles). **h** A cartoon of the band diagram of the bottom surface of the TI as the temperature is decreased at a fixed gate voltage. Error bars represent an uncertainty with 95% confidence

using a two-channel model:

$$\Delta\sigma(H) = \sum_{i=0,1} a_i \frac{e^2}{2\pi^2\hbar} \left[\psi\left(\frac{1}{2} + \frac{\hbar c}{4el_{\phi,i}^2 H}\right) - \ln\left(\frac{\hbar c}{4el_{\phi,i}^2 H}\right) \right], \alpha_0 = -1/2. \quad (1)$$

Here $l_{\phi,i}$ and a_i are the dephasing length and prefactors respectively, corresponding to the topmost gapless surface state ($i = 0$) and the bottom gapped surface state with $i = 1$. We fitted the MC data using three parameters, $l_{\phi,0}$, $l_{\phi,1}$, and a_1 , fixing $a_0 = -1/2$. Note that, for the purposes of our analysis, we neglect corrections to the dephasing length $l_{\phi,1}$ since this would introduce additional fitting parameters. (See Supplementary S4 for examples of fits to the data.) The prefactor a_1 corresponds to the quantum corrections to the MC of the bottom surface and provides an indirect way to estimate the chemical potential in this surface state as it is varied with gate voltage. Figure 3d, e show that a_1 increases as the gate voltage decreases from $V_G = 1$ V to

$V_G = -5$ V (-7 V) at 0.1 K (0.29 K). We attribute this behavior to E_F at the bottom surface being tuned from the conduction band down toward the magnetic gap but not passing through it as illustrated in Fig. 3f. This qualitatively agrees with the WAL–WL crossover when the Berry phase changes from π to a smaller value by tuning E_F . Similarly, if we fix $V_G = -5$ V to place E_F close to the gap and vary the temperature, a_1 increases with decreasing temperature (Fig. 3g): this occurs because Δ increases at lower temperatures due to the temperature dependence of the interfacial exchange coupling with the adjacent (Ga,Mn)As layer (illustrated in Fig. 3h). An unexplained feature of our results is the range of values obtained for a_1 . Based on theory,⁴⁶ we would anticipate that $0 \leq a_1 \leq 1$ as the ratio Δ/E_F varies from zero (at high temperature or at large positive gate voltage) to large (at low temperature or at negative gate voltage). Instead, fits to the data yield $0.4 \leq a_1 \leq 0.7$. This likely points to oversimplification in our two-channel model and suggests that inter-channel scattering probably needs to be considered.

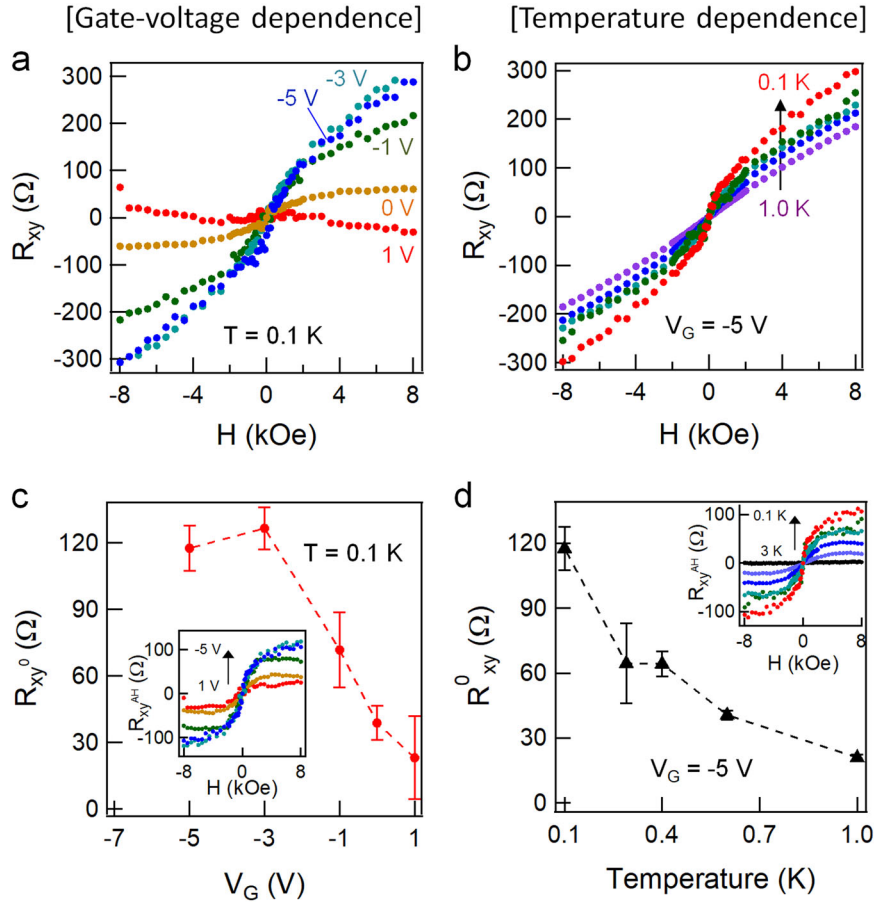


Fig. 4 Anomalous Hall effect. **a** Magnetic field dependence of the Hall resistance R_{xy} at different V_G at $T = 0.1$ K. The slope changes sign, indicating a change in carrier type from n- to p-type as the gate voltage is varied. **b** Magnetic field dependence of the Hall resistance R_{xy} at $T \leq 1.0$ K at fixed V_G , showing that the AHE becomes more pronounced as temperature decreases. **c** Gate-voltage dependence of the magnitude of the anomalous Hall resistance R_{xy}^0 at $T = 0.1$ K (red circles). The inset shows the anomalous Hall resistance R_{xy}^{AH} at different V_G : 1 V (red), 0 V (orange), -1 V (green), -3 V (cyan), and -5 V (blue). **d** Temperature dependence of R_{xy}^0 with $V_G = -5$ V. The inset shows R_{xy}^{AH} at $T = 3.0$ K (black), 1.0 K (violet), 0.6 K (blue), 0.4 K (cyan), 0.29 K (green), and 0.1 K (red). Error bars represent an uncertainty with 95% confidence

Anomalous Hall effect

We now discuss the results from Hall measurements where we observe a systematic emergence of non-linear magnetic field dependence of the Hall resistance as the chemical potential is lowered at a fixed temperature by varying the gate voltage (Fig. 4a, c) or as the temperature is decreased at a fixed gate voltage (Fig. 4b, d). We note that, over the range of temperature studied (a few K), the chemical potential of the top and bottom surfaces does not change much at a fixed gate voltage, suggesting that the non-linear Hall effect is unlikely to arise from two channels with different carrier densities and mobilities. A more consistent interpretation attributes this behavior to the AHE and prompts us to study the effect of a finite energy gap on the Hall conductance. The absence of hysteresis of the AHE indicates that long-range magnetic ordering is not induced in the bottom surface of the TI film by the adjacent (Ga,Mn)As layer in the measurement range of temperature (100 mK–10 K) and gate voltage (-7 to 1 V). To understand the anomalous Hall contribution from the interface between TI and FMI, we consider a two-dimensional Dirac model with a finite energy gap (Δ). A direct calculation of the Hall conductance leads to

$$\sigma_{xy} \left(-\frac{|\Delta|}{2} < E_F < \frac{|\Delta|}{2} \right) = \frac{e^2}{2h}, \sigma_{xy} \left(E_F > \frac{|\Delta|}{2} \right) = \frac{e^2}{2h} \frac{\Delta}{2E_F} \quad (2)$$

with $E_F = \sqrt{(\hbar v_F k)^2 + (\Delta/2)^2}$. (See Supplementary Information S5

for detailed calculations). Equation (2) shows that the Hall conductivity is half-quantized in the insulating regime of a single Dirac model, and the half-integer quantum Hall conductivity monotonically decreases as E_F moves above the energy gap or as the gap gradually closes with an E_F fixed to a position near the gap.

Since our results are not in the regime of the quantized Hall conductivity, the observed Hall conductivity is smaller than $e^2/2h$. However, it follows the qualitative behavior of Eq. (2). Figure 4c, d (insets) clearly show the systematic emergence of the anomalous Hall term R_{xy}^{AH} with respect to the gate voltage and temperature, where R_{xy}^{AH} is obtained after subtracting the ordinary Hall term R_{xy}^{OH} from the Hall resistance as $R_{xy}^{AH} = R_{xy} - R_{xy}^{OH}$. We show R_{xy}^{AH} instead of σ_{xy}^{AH} since R_{xx} term contains a large contribution of the top surface and affects the values of $\sigma_{xy} = R_{xy} / (R_{xx}^2 + R_{xy}^2)$. The expression for R_{xy} from σ_{xy} can be written as:

$$R_{xy} \left(E_F > \frac{|\Delta|}{2} \right) = \frac{\sigma_{xy}}{\sigma_{xx}^2 + \sigma_{xy}^2} \cong \frac{m^2}{2\hbar e^2 \tau^2} \frac{1}{n^2} \frac{\Delta}{2E_F} \quad (3)$$

with σ_{xx} from the Drude model $\sigma_{xx} = e^2 \tau n / m$ where n , m , and τ are, respectively, the carrier density, the effective mass, and the relaxation time between collisions. For $E_F > |\Delta|/2$, n increases as E_F increases (moves away from the gap). Similarly to the case of quantum corrections to MC, the change of R_{xy} reveals a systematic

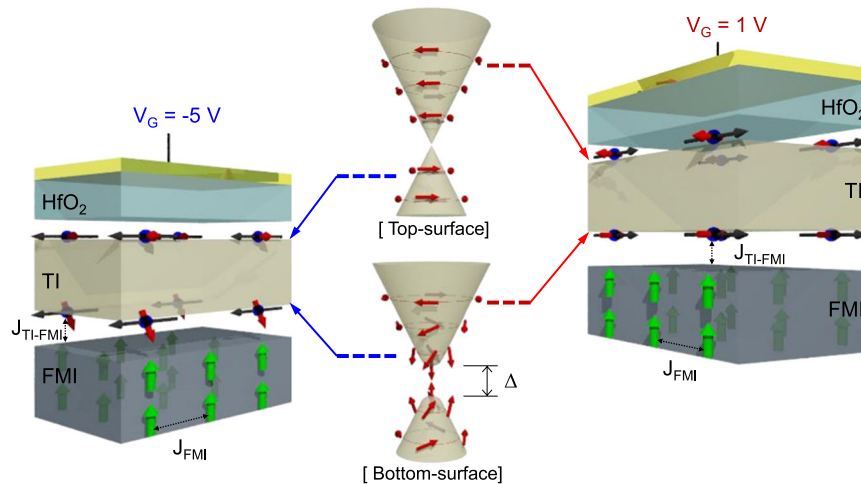


Fig. 5 Spin textures in TI surfaces. An illustration of a gapless Dirac surface state for the top surface, a magnetically gapped surface state with hedgehog spin texture for the bottom surface, and top-gated TI/(Ga,Mn)As heterostructure devices with $V_G = -5$ V and $V_G = +1$ V. Green arrows represent the magnetization of the (Ga,Mn)As layer and gray and red arrows in the TI layer represent the directions of electron propagation and its spin, respectively. J_{FMI} is the exchange-coupling constant between Mn moments in (Ga,Mn)As while $J_{\text{TI-FMI}}$ is the weaker exchange-coupling constant between electrons in the TI bottom surface and Mn moments in (Ga,Mn)As

modification of the size of the energy gap and the chemical potential. As the chemical potential lowers and approaches the energy gap by tuning the gate voltage from 1 to -5 V, the estimated magnitude of the anomalous Hall resistance R_{xy}^0 increases. R_{xy}^0 is the intercept obtained by extrapolating a linear line of the high field Hall resistance. R_{xy}^0 is zero in the case of a closed gap ($\Delta = 0$). When a gap opens and widens, a non-zero R_{xy}^0 monotonically increases. Figure 4c shows the evolution of the anomalous Hall resistance R_{xy}^0 as the chemical potential lowers toward the energy gap. Similarly, Fig. 4d shows a monotonic increase of R_{xy}^0 with decreasing temperature, interpreted as the widening of the gap with decreasing temperature. The interpretation of both gate-voltage dependence and temperature dependence of the AHE is consistent with that of the quantum corrections to the MC with varying gate voltage and temperature. The onset temperature of both AHE and WL is much lower than the T_C of the adjacent (Ga,Mn)As layer, indicating that the exchange coupling between electrons in TI bottom surface and Mn moments in (Ga,Mn)As is much weaker than the exchange coupling between Mn moments in (Ga,Mn)As (Fig. 5).

In summary, we synthesized and characterized a heterostructure of a TI film $(\text{Bi,Sb})_2(\text{Te,Se})_3$ on a ferromagnetic semiconductor (Ga,Mn)As. The $\text{Ga}_{0.95}\text{Mn}_{0.05}\text{As}$ layer is highly resistive with a perpendicular component of magnetization below 50 K. With an optimal Bi-to-Sb ratio, the chemical potential was placed in the surface state and further tuned by electrical top gating. We observed a crossover between WAL and WL, as well as the systematic emergence of the AHE with varying temperature and gate voltage, interpreted as a result of a gap opening in the Dirac surface state due to the TR symmetry breaking by the exchange coupling between the TI surface state and the adjacent (Ga,Mn)As. The results suggest that the systematic changes in MC and AHE can be used as indirect probes to estimate the position of the chemical potential E_F and the opening of a magnetic gap in the surface state. Our study also identifies a valuable new model quantum material for systematic explorations of topological phenomena in the presence of broken TR symmetry. A full exploitation of this platform will require optimization of the TI/(Ga, Mn)As interface, a key measure of which would be the observation of a robust hysteresis in the AHE.

METHODS

Experimental techniques

Longitudinal resistance of a top-gated $(\text{Bi,Sb})_2(\text{Te,Se})_3/(\text{Ga,Mn})\text{As}$ Hall-bar device (above 0.29 K) was measured as a function of gate voltage and temperature in an Oxford Heliox Helium-3 cryostat inserted into a liquid Helium dewar equipped with a superconducting magnet. Magneto-transport measurements at temperatures < 0.29 K were carried out using a dilution refrigerator in a Physical Property Measurement System from Quantum Design. Longitudinal channel resistance and Hall resistance were simultaneously measured using standard lock-in technique with an alternating current excitation current of 200 nA and a low frequency of 19 Hz.

Magnetization measurements of the $(\text{Bi,Sb})_2(\text{Te,Se})_3/(\text{Ga,Mn})\text{As}$ heterostructure were performed using a Quantum Design superconducting quantum interference device. A magnetic field perpendicular to the sample surface was applied to investigate the perpendicular component of magnetization, revealing a Curie temperature of 50 K.

For microstructural characterization, a cross-sectional lamella of a top-gated Hall-bar device of the $(\text{Bi,Sb})_2(\text{Te,Se})_3/(\text{Ga,Mn})\text{As}$ heterostructure was prepared by a focused ion beam (FEI Quanta 200 3D). The lamella was cleaned in an oxygen plasma cleaner to minimize contamination and then transferred into an FEI Titan G2 TEM system. High-angle annular dark field scanning TEM was used for structural analysis of the $(\text{Bi,Sb})_2(\text{Te,Se})_3/(\text{Ga, Mn})\text{As}$ heterostructure, and chemical information of elemental composition of each layer as well as elemental mapping of the whole structure was characterized by EDS.

DATA AVAILABILITY

The data that support the findings of this study are available from the corresponding author upon reasonable request.

ACKNOWLEDGEMENTS

This work was supported in part by DARPA and C-SPIN, one of the six centers of STARnet, a Semiconductor Research Corporation program, sponsored by MARCO and DARPA. N.S. and A.R. acknowledge additional support from ONR grant N00014-15-1-2370 and C.-x.L. from ONR grant N00014-15-1-2675 and ONR renewal No. N00014-18-1-2793).

AUTHOR CONTRIBUTIONS

J.S.L., A.R., and N.S. conceived the project. J.S.L. conducted material characterization, device fabrication, and transport measurements. A.R. synthesized the material. A.R. and R.D.F. conducted SQUID measurements. C.-x.L. performed the numerical calculation. J.S.L. and C.-x.L. analyzed the results. W.Z. helped with transport

measurements. J.S.L and N.S. wrote the manuscript. All authors discussed the results and contributed to the final manuscript.

ADDITIONAL INFORMATION

Supplementary information accompanies the paper on the *npj Quantum Materials* website (<https://doi.org/10.1038/s41535-018-0123-2>).

Competing interests: The authors declare no competing interests.

Publisher's note: Springer Nature remains neutral with regard to jurisdictional claims in published maps and institutional affiliations.

REFERENCES

- Moore, J. E. The birth of topological insulators. *Nature* **464**, 194–198 (2010).
- Hasan, M. & Kane, C. Colloquium: topological insulators. *Rev. Mod. Phys.* **82**, 3045–3067 (2010).
- Qi, X.-L. & Zhang, S.-C. The quantum spin Hall effect and topological insulators. *Phys. Today* **63**, 33–38 (2010).
- Fu, L., Kane, C. L. & Mele, E. J. Topological insulators in three dimensions. *Phys. Rev. Lett.* **98**, 106803 (2007).
- Qi, X.-L., Hughes, T. L. & Zhang, S.-C. Topological field theory of time-reversal invariant insulators. *Phys. Rev. B* **78**, 195424 (2008).
- Liu, Q., Liu, C.-X., Xu, C., Qi, X.-L. & Zhang, S.-C. Magnetic impurities on the surface of a topological insulator. *Phys. Rev. Lett.* **102**, 156603 (2009).
- Chen, Y. L. et al. Massive Dirac fermion on the surface of a magnetically doped topological insulator. *Science* **329**, 659–662 (2010).
- Wray, L. A. et al. A topological insulator surface under strong Coulomb, magnetic and disorder perturbations. *Nat. Phys.* **7**, 32–37 (2011).
- Qi, X.-L., Li, R., Zang, J. & Zhang, S.-C. Inducing a magnetic monopole with topological surface states. *Science* **323**, 1184–1187 (2009).
- Yu, R. et al. Quantized anomalous Hall effect in magnetic topological insulators. *Science* **329**, 61–64 (2010).
- Chang, C.-Z. et al. Experimental observation of the quantum anomalous Hall effect in a magnetic topological insulator. *Science* **340**, 167–170 (2013).
- Wu, L. et al. Quantized Faraday and Kerr rotation and axion electrodynamics of a 3D topological insulator. *Science* **354**, 1124–1127 (2016).
- Mogi, M. et al. Tailoring tricolor structure of magnetic topological insulator for robust axion insulator. *Sci. Adv.* **3**, aao1669 (2017).
- Xiao, D. et al. Realization of the axion insulator state in quantum anomalous hall sandwich heterostructures. *Phys. Rev. Lett.* **120**, 056801 (2018).
- Checkelsky, J. G., Ye, J., Onose, Y., Iwasa, Y. & Tokura, Y. Dirac-fermion-mediated ferromagnetism in a topological insulator. *Nat. Phys.* **8**, 729–733 (2012).
- Zhang, J. et al. Topology-driven magnetic quantum phase transition in topological insulators. *Science* **339**, 1582–1586 (2013).
- Lee, J. S. et al. Ferromagnetism and spin-dependent transport in n-type Mn-doped bismuth telluride thin films. *Phys. Rev. B* **89**, 174425 (2014).
- Zhang, D. et al. Interplay between ferromagnetism, surface states, and quantum corrections in a magnetically doped topological insulator. *Phys. Rev. B* **86**, 205127 (2012).
- Choi, Y. H. et al. Transport and magnetic properties of Cr-, Fe-, Cu-doped topological insulators. *J. Appl. Phys.* **109**, 07E312 (2011).
- Song, Y. R. et al. Large magnetic moment of gadolinium substituted topological insulator: $\text{Bi}_{1.98}\text{Gd}_{0.02}\text{Se}_3$. *Appl. Phys. Lett.* **100**, 242403 (2012).
- Chang, C.-Z. et al. Chemical-potential-dependent gap opening at the Dirac surface states of Bi_2Se_3 . *Phys. Rev. Lett.* **112**, 056801 (2014).
- Sanchez-Barriga, J. et al. Nonmagnetic band gap at the Dirac point of the magnetic topological insulator $(\text{Bi}_{1-x}\text{Mn}_x)_2\text{Se}_3$. *Nat. Commun.* **7**, 10559 (2016).
- Xu, S.-Y. et al. Hedgehog spin texture and Berry's phase tuning in a magnetic topological insulator. *Nat. Phys.* **8**, 616–622 (2012).
- Pesin, D. & MacDonald, A. H. Spintronics and pseudospintronics in graphene and topological insulators. *Nat. Mater.* **11**, 409–416 (2012).
- Mellnik, A. R. et al. Spin-transfer torque generated by a topological insulator. *Nature* **511**, 449–451 (2014).
- Deorani, P. et al. Observation of inverse spin Hall effect in bismuth selenide. *Phys. Rev. B* **90**, 094403 (2014).
- Jamali, M. et al. Giant spin pumping and inverse spin Hall effect in the presence of surface and bulk spin-orbit coupling of topological insulator Bi_2Se_3 . *Nano. Lett.* **15**, 7126–7132 (2015).
- Li, C. H. et al. Electrical detection of charge-current-induced spin polarization due to spin-momentum locking in Bi_2Se_3 . *Nat. Nanotechnol.* **9**, 218–224 (2014).
- Lee, J. S., Richardella, A., Hickey, D. R., Mkhoyan, K. A. & Samarth, N. Mapping the chemical potential dependence of current-induced spin polarization in a topological insulator. *Phys. Rev. B* **92**, 155312 (2015).
- Wei, P. et al. Exchange-coupling-induced symmetry breaking in topological insulators. *Phys. Rev. Lett.* **110**, 186807 (2013).
- Yang, Q. I. et al. Emerging weak localization effects on a topological insulator/insulating ferromagnet (Bi_2Se_3 -EuS) interface. *Phys. Rev. B* **88**, 081407(R) (2013).
- Kandala, A. et al. Growth and characterization of hybrid insulating ferromagnet-topological insulator heterostructure devices. *Appl. Phys. Lett.* **103**, 202409 (2013).
- Alegria, L. D. et al. Large anomalous Hall effect in ferromagnetic insulator-topological insulator heterostructures. *Appl. Phys. Lett.* **105**, 053512 (2014).
- Yang, W. et al. Proximity effect between a topological insulator and a magnetic insulator with large perpendicular anisotropy. *Appl. Phys. Lett.* **105**, 092411 (2014).
- Jiang, Z. et al. Enhanced spin Seebeck effect signal due to spin-momentum locked topological surface states. *Nat. Commun.* **7**, 11458 (2016).
- Katmis, F. et al. A high-temperature ferromagnetic topological insulating phase by proximity coupling. *Nature* **533**, 513–516 (2016).
- Wang, H. et al. Surface-state-dominated spin-charge current conversion in topological-insulator-ferromagnetic-insulator heterostructures. *Phys. Rev. Lett.* **117**, 076601 (2016).
- Zheng, G. et al. Tunable Dirac fermion dynamics in topological insulators. *Sci. Rep.* **6**, 21334 (2016).
- Tang, C. et al. Above 400-k robust perpendicular ferromagnetic phase in a topological insulator. *Sci. Adv.* **3**, e1700307 (2017).
- Neupane, M. et al. Observation of quantum-tunnelling-modulated spin texture in ultrathin topological insulator Bi_2Se_3 films. *Nat. Commun.* **5**, 3841 (2014).
- MacDonald, A., Schiffer, P. & Samarth, N. Ferromagnetic semiconductors: moving beyond (Ga,Mn)As. *Nat. Mater.* **4**, 195–202 (2005).
- Ku, K. C. et al. Highly enhanced Curie temperature in low-temperature annealed (Ga,Mn)As epilayers. *Appl. Phys. Lett.* **82**, 2302 (2003).
- Matsukura, F., Sawicki, M., Dietl, T., Chiba, D. & Ohno, H. Magnetotransport properties of metallic (Ga,Mn)As films with compressive and tensile strain. *Phys. E* **21**, 1032–1036 (2004).
- Richardella, A. et al. Coherent heteroepitaxy of Bi_2Se_3 on GaAs (111)B. *Appl. Phys. Lett.* **97**, 262104 (2010).
- Chen, C. et al. Tunable Dirac fermion dynamics in topological insulators. *Sci. Rep.* **3**, 2411 (2013).
- Lu, H.-Z., Shi, J. & Shen, S.-Q. Competition between weak localization and antilocalization in topological surface states. *Phys. Rev. Lett.* **107**, 76801 (2011).
- Lang, M. et al. Competing weak localization and weak antilocalization in ultrathin topological insulators. *Nano. Lett.* **13**, 48–53 (2013).
- Bao, L. et al. Quantum corrections crossover and ferromagnetism in magnetic topological insulators. *Sci. Rep.* **3**, 2391 (2013).
- Cha, J. J. et al. Effects of magnetic doping on weak antilocalization in narrow Bi_2Se_3 nanoribbons. *Nano. Lett.* **12**, 4355–4359 (2012).
- Liu, M. et al. Crossover between weak antilocalization and weak localization in a magnetically doped topological insulator. *Phys. Rev. Lett.* **108**, 036805 (2012).
- Zhang, Z. et al. Electrically tuned magnetic order and magnetoresistance in a topological insulator. *Nat. Commun.* **5**, 4915 (2014).



Open Access This article is licensed under a Creative Commons Attribution 4.0 International License, which permits use, sharing, adaptation, distribution and reproduction in any medium or format, as long as you give appropriate credit to the original author(s) and the source, provide a link to the Creative Commons license, and indicate if changes were made. The images or other third party material in this article are included in the article's Creative Commons license, unless indicated otherwise in a credit line to the material. If material is not included in the article's Creative Commons license and your intended use is not permitted by statutory regulation or exceeds the permitted use, you will need to obtain permission directly from the copyright holder. To view a copy of this license, visit <http://creativecommons.org/licenses/by/4.0/>.

© The Author(s) 2018